MODELLING RESULTS OF LIQUEFACTION TESTS ON A NONPLASTIC SILT

Devrim Erdoğan[1*],   Nazar Tanrınıan[2],   Alper Sezer[3],   Eyyüb Karakan[4]

[1]Assist. Prof. Dr. Ege Univ. Civil Engineering Dept.; devrim.sufa.erdogan@ege.edu.tr; devrim.ulgen@gmail.com

[2]M.Sc DNV GL Corporation, Civil Engineer, ntanrinian@gmail.com

[3]Assoc.Prof.Dr. Ege Univ. Civil Engineering Dept, alper.sezer@ege.edu.tr

[4]Assist.Prof.Dr. Kilis Univ. Civil Engineering Dept. eyyubkarakan@gmail.com

[*]Corresponding Author

RESEARCH ARTICLE – ENGLISH

Abstract

Liquefaction is simply defined as the sudden increase in pore water pressure as a result of cyclic loading, which causes excessive ground settlements and damage in overlying or buried structures. Many studies in literature focused on evaluation of liquefaction susceptibility. These methods can be classified as a) stress-based b) strain based c) energy based methods d) numerical modelling based analysis and e) Arias-intensity based methods. In this study, an alternative approach for assessment of liquefaction susceptibility is aimed by use of clustering algorithms. In this regard, results of 54 cyclic triaxial tests results on a nonplastic silt including post-liquefaction volume changes was used for evaluation and classification of liquefaction behavior after cyclic triaxial testing. In the experimental part, specimens prepared at increasing relative densities between 30% and 80%, at a step of 10% were consolidated under 100 kPa effective confining pressure. The results revealed that, unsupervised clustering algorithms are reliable tools in classification of liquefaction state and post-liquefaction volumetric strains of nonplastic silts. In this regard, cyclic stress ratio and number of cycles are useful inputs for classification of liquefaction state. In addition, cyclic stress ratio, number of cycles, pore water pressure ratio and cyclic axial strain can be used to classify the post-liquefaction volumetric strains. Use of ANFIS depending on combinations of cyclic stress ratio, number of cycles, pore water pressure ratio, initial relative density and cyclic axial strain end up with promising results in estimation of post-liquefaction volumetric strain, however, these parameters are far from modelling factor of safety to liquefaction.

Keywords: Hard k-means classifier; fuzzy c-means algorithm; self-organizing maps; ANFIS, liquefaction; silt; cyclic triaxial tests

Nonplastik Silt Üzerinde Gerçekleştirilen Sıvılaşma Deneylerinin Modellenmesi

Özet

Sıvılaşma, çevrimsel yükleme sırasında boşluksuyu basıncında meydana gelen ani yükselmesi sonucunda zeminin kayma dayanımında kayda değer düşüşlerin ve buna bağlı olarak yüksek düzeylerde oturmalar ve üst yapıda da hasarın meydana geldiği bir olgudur. Literatürde zeminlerin sıvılaşabilirlikleri a) gerilme tabanlı b) deformasyon tabanlı c) energy tabanlı d) sıvılaşma bünye modellerinin kullanıldığı sayısal modelleme teknikleri ve e) Arias yoğunluğu yöntemleri ile belirlenebilmektedir. Bu çalışmada, sıvılaşabilirliğin belirlenebilmesi için sınıflandırma (clustering) algoritmaları kullanılmıştır. Bu amaçla, non-plastik silt üzerinde yapılmış olan 54 tane dinamik üç eksenli basınç deneyinin sonuçları kullanılmıştır. Bu deney sonuçları sıvılaşma sonrası oturma verilerini de kapsamaktadır. Deneyler, sıkılığı 30% ile 80% arasında 10% aralıklarla değişen ve 100 kPa altında konsolide edilmiş non-plastik silt örnekleri üzerinde gerçekleştirilmiştir. Analiz sonuçlarına göre, eğitimsiz sınıflandırma algoritmaları, non-plastik silt örneklerinin sıvılaşabilirliklerinin ve sıvılaşma sonrası hacimsel birim deformasyonlarının belirlenmesinde etkili bir teknik olarak karşımıza çıkmaktadır. Buna göre, çevrimsel gerilme oranı ve çevrim sayısı parametrelerinin sıvılaşma durumunun belirlenmesinde uygun girdiler olduğu görülmektedir. Öte yandan, çevrimsel gerilme oranı, çevrim sayısı, aşırı boşluksuyu basıncı oranı, çevrimsel eksenel birim deformasyon parametrelerinin ise sıvılaşma sonrası hacimsel birim deformasyonların sınıflandırılmasında etkili parametreler oldukları görülmektedir. Çevrimsel gerilme oranı, çevrim sayısı, aşırı boşluksuyu basıncı oranı, sıkılık ve çevrimsel eksenel birim deformasyon parametrelerinin kombinasyonundan oluşan ANFIS'in kullanımı sıvılaşma sonrası hacimsel birim deformasyonların tahmin edilmesinde kayda değer bir rol oynarken, bu parametreler sıvılaşmaya karşı güven sayısının tahmininde zayıf kalmaktadırlar.

Anahtar kelimeler: K ortalamaları yöntemi; Bulanık c ortalamaları yöntemi; Kendini ayarlayabilen haritalar; ANFIS (Uygulamalı ağ tabanlı bulanık çıkarım sistemi), Sıvılaşma; silt; Dinamik üç eksenli basınç deneyi.

1. Introduction

Liquefaction is one of the most important phenomenon in geotechnical engineering, and is responsible for the loss of many lives accompanying with a substantial damage in building stock and buried structures (Karakan et al., 2019a; 2019b). In the past, engineers used many methods to assess the vulnerability of soil to ground motions, particularly for assessment of liquefaction phenomenon. In this regard, a comparison of cyclic stress ratio (CSR) with cyclic resistance ratio (CRR) is a relatively easy method, which enables to compare the applied seismic load with soil resistance or capacity. The ratio of these two parameters give us a factor of safety against liquefaction, and empirical / experimental methods for determination of CSR and CRR attracted the attention of geotechnical engineers (Seed et al. 1985; Andrus and Stokoe 2000; Boulanger and Idriss 2014). A number of methods including a) Stress-based approach (Seed and Idriss, 1971), strain-based approach (Dobry, 1982), energy-based approach (Zhang et al., 2015), numerical modelling analysis (Seed and Idriss, 1969), and Arias intensity approach (Kayen and Mitchell, 1997) were employed to provide alternative means for determination of factor of safety, for practical use.

Classified in terms of a transition material, silt size is between those of clay and sand. It is not correctly understood whether chemical or mechanical effects control the behaviour of these soils, and more effort is needed to understand the complex mechanism governing the index, compression and mechanical properties of this soil type. In the last few decades, several studies are performed to assess the liquefaction properties of silts (Karakan et al., 2018a; 2018b

Thevanayagam et al. (2000) have studied extensively the effect of fines content on the liquefaction resistance of sand–non-plastic fines mixtures and recommends the use of intergranular void ratio for the interpretation of the experimentally observed behavior. It is worth mentioning, that the importance of this parameter had already been recognized by Kenny (1977). More specifically, Thevanayagam et al. (2000) proposed a conceptual framework in which the soil mixture is assumed to be composed of spherical particles having two different diameter values, coarse grains and fine grains. Taking into account possible interactions between coarser and finer grains the intergranular, and interfine, void ratios are introduced as primary indices of contact density for granular mixtures with low and high fine grain contents. Furthermore, laboratory tests show that at similar void ratio and confining stress, the presence of fines up to at least about 25% of the total weight decreases the liquefaction cyclic strength (Xenaki and Athanasopoulos, 2003; Papadopoulou and Tika, 2008). Recently, the effects of both the consolidation stress and void ratio on the liquefaction cyclic strength has been simulated by only one

parameter, the state parameter, defined hereunder (Chen and Liao, 1999; Stamatopoulos and Balla, 2004). It has been observed that the relationship between the state parameter and the liquefaction cyclic strength for soil samples with different fines content tested in the triaxial device is unique for the same sample preparation method (Stamatopoulos, 2010) and differs for different sample separation methods (Qadimia and Mohammadi, 2014).

Cyclic liquefaction behavior has been extensively studied for clean sands (Boulanger 2003; Yoshimine and Koike 2005) and sandy soils with less than 35% silt content (Polito and Martin, 2001; Xenaki and Athanasopoulos, 2003; Carraro et al., 2003; Stamatopoulos, 2010), and the existing relationships for liquefaction analysis and the estimation of cyclic resistance of non-plastic soils are often applicable for silty sands with less than 30% silt content (Idriss and Boulanger, 2008). Very little work has been conducted on the liquefaction potential and cyclic shearing behavior of non-plastic silts and sandy silts partly due to the biased perception that fine-grained soils have lower potential to develop excess pore water pressure compared to sands (Jurko et al., 2006).

Generally, in uniform non-plastic soils, such as sand or silt, only the generated pore water pressure and arrangement of grains can affect the post-cyclic strength. Since soil arrangement depends on grain shape, which is in turn a material parameter, both decrease (Yoshida et al, 1994) and increase (Vaid and Thomas, 1995) in strength and stiffness after applying cyclic load have been reported (Yasuhara et al., 2005). Due to the bonding forces between soil

particles and the overall structure effect (Sorensen et al., 2007), the post-cyclic behaviour of cohesive soil exhibits more complexly than sand (Yasuhara et al., 1992). For normally consolidated cohesive soil, Hyde et al. (2007) indicated that the soil skeleton of remoulded silt will be densified after post-cyclic reconsolidation and the post drainage cyclic strength of it will increase with initial anisotropically consolidated ratio, however, this silt can still be liquefied by aftershocks. Comparing undrained shear behaviour between pre- and post-cyclic loading, Wang et al. (2015) found that the shear strength and stiffness of Mississippi River silt rise steadily with an increase of the degree of reconsolidation and the slopes of CSL of silt before and after cyclic loading are different due to the change in the microstructure of silt.

Repeated loading in loose soils, can cause recompression and an increase in soil resistance, whereas in dense soils, repeated loading can result in increase of soil deformation, as seen by many researchers (Yasuhara and Andersen 1991; O'Reilly et al. 1991). It is not difficult to relate the recompression to the rise in pore pressure and shear strain. For example, Hyde et al. (2007), Wijewickreme and Sanin (2010), and Yasuhara and Andersen (1991) related recompression to the pore pressure and strain developed in the soil and observed that it was not influenced by CSR alone, but also the number of load cycles

Investigations on post-liquefaction behavior of sands also proved that strength and stiffness of soils are significanltly reduced after liquefaction. But as axial strain increases, sand grains gradually reach a stable condition under the new arrangement. Hereafter specimen shows dilative behavior, both strength and stiffness increase (Yoshida et al, 1994). In this case, the post-cyclic behavior of sand specimens significantly depends on maximum strain and pore water pressure induced by cyclic loading (Vaid and Thomas, 1995).

On the other hand, unsupervised clustering algorithms are versatile tools for classification of data in n-dimensional space. By minimizing the Euclidean distances to predefined cluster centers, these algorithms cluster data based on an iterative approach. In the past, many attempts were made to classify geotechnical data by use of these algorithms. In this regard, Hanesch et al. (2001) made an attempt to determine polluted areas based on geological data by using fuzzy c-means algorithm and nonlinear mapping methodology. Zhang and Tumay (2003) presented a soil classification system establishing a link among soil composition and mechanical behaviour of soils. Studying on GPR data, Odhiambo et al. (2004) used fuzzy c-means classifier for soil classification. Young and Hammer (2000) used these classifiers for identifying pedologically and geographically distinct groups. The authors emphasize that, cluster analysis seems to be useful for revealing homogenous soil patterns and identifying the link among soil properties and landforms. Goktepe at al. (2005; 2007) utilized unsupervised clustering algorithms for soil classification as well as the change in time-dependent strength. Hot and Popovic-Bugarin (2016) employed these classifiers for pedologic mapping, the authors stress that two types of soils dominate Montenegro. Aidona et al. (2016)

used hierarchical cluster analysis to classify Thessaloniki soils in terms of their magnetic properties. Further attempts were also made by Shi et al. (2016) and Lu et al. (2017) utilized FCM for analysis of debris flow susceptibility and mapping soil texture, respectively. Song et al. (2017) performed analyses with an improved FCM method for identification of rock discontinuity sets. Viviescas et al. (2019) employed hierarchical clustering for evaluation of soil undrained based on SPT data.

Adaptive neuro-fuzzy inference systems (ANFIS) is a popular and fruitful method for establishing link between input and output mapping of n-dimensional data. ANFIS simply unifies the linguistic variables of a fuzzy system with learning feature of Artificial Neural Networks (ANNs). In the past, a vast of amount of studies were used to classify the soils using ANFIS. Gokceoglu et al. (2003) used ANFIS for estimation of deformation modulus of rock masses. Provenzano et al. (2004) made an attempt to predict response of a model footing subjected to vertical centered and eccentric loads using ANFIS. Kayadelen et al. (2009) performed a study concerning friction angle estimation. The authors stress that developed ANFIS models, are capable of learning the complex relationship among several index properties (fines content, liquid limit, density) and friction angle. The paper by Rangel et al. (2005) presents an alternative approach to evaluate the tunnel stability during construction using a Neuro-Fuzzy system. Sezer (2013) used ANFIS for prediction of permeability of granular soils. Additional studies in geotechnical engineering applications using ANFIS was conducted for estimation of permeability (Tayfur et al. 2014), deformation modulus of rock mass (Fattahi, 2016), unsaturated soil strength (Jokar and Mirasi, 2018), groutability of granular soils (Tekin and Akbas, 2019), bearing capacity (Moayedi and Rezai, 2020), load settlement behaviour of raft foundations (Liu et al., 2020).

A short literature survey above revealed that a classification or an ANFIS-modelling attempt based on liquefaction data was not performed before. Therefore, this study aims to classify liquefaction susceptibility and post-liquefaction volumetric strains of nonplastic silts, based on a series of cyclic triaxial tests. Classification results along with ANFIS modelling attempts revealed that, there is a potential of estimation of liquefaction susceptibility and post-liquefaction volumetric strains by use of these algorithms.

2. Materials and Methods

2.1. Properties of Silt

The non-plastic silt used in this study was obtained from ESAN company. The silt has a specific gravity of 2.65. The grain size distribution of silt is given in Figure 1. The maximum and minimum void ratios in accordance with related ASTM standards were determined as 1.352 and 0.894, respectively (ASTM, 2016a; 2016b).

2.2. Cyclic Triaxial Tests

An experimental program was prepared to investigate interrelationships among initial relative density, cyclic stress ratio (CSR), number of cycles, pore water pressure ratio, double amplitude of axial strain, post liquefaction volumetric strain and factor of safety. For this aim,

stress-controlled cyclic triaxial tests were per-formed using a DTC-S367 cyclic triaxial system purchased from Seiken Inc. The system consists of vertical pressure loading unit with air and water panel, triaxial cell, pneumatic sine loader, an electric measurement unit including, pressure & displacement transducers & volume change transducer, strain amplifiers, and dynamic data acquisition system. The servo reservoir assembly includes a regulator for setting the required pressure, a reservoir to smooth out any changes in the air supply pressure, two water traps and two pneumatic servo valves are used for controlling confining and back pressures. Distribution panel controls all water flow, automatic volume change apparatus and the triaxial cell. The cyclic triaxial apparatus is equipped with a single column load frame, with a servo-pneumatic actuator with external displacement transducer. The high performance servo valve provides a sinusoidal vibration frequency between 0.001 to 10 Hz. Axial displacement is measured by means of a displacement transducer with a travel distance of 50 mm. axial load is monitored using a bellofram cylinder type of load cell with a capacity of 2 kN, which is mounted inside the triaxial cell. Thus, it only measures the vertical loads applied to the specimen and a possible falsification of the measured values of vertical load due to piston friction is avoided. The transparent acrylic cylinder of the triaxial cell has a working pressure of 1 MPa. A double burette type volume change apparatus was located in the system that contains a transducer with a stroke of 25 ml to measure the volume changes of saturated specimens (Karakan et al. 2019a, b).
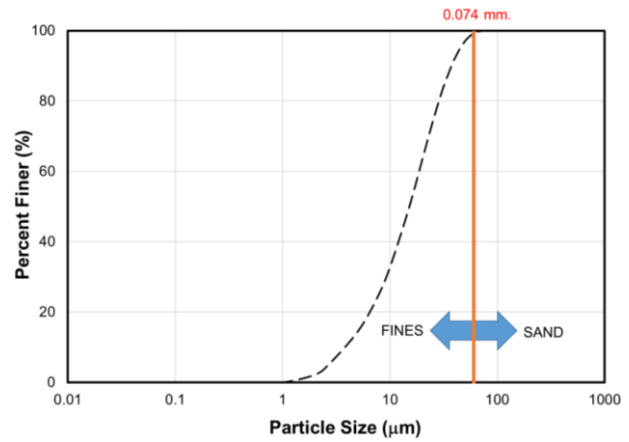

Figure 1. Grain size distribution of nonplastic silt

The experiments were performed on specimens of 50 mm x 100 mm dimensions (diameter x height). JGS 0520-2000 was the guide in preparation of specimens and tests were performed in accordance with JGS 0541-2000. A porous stone and a filter paper were placed on pedestal. Attaching a cylindrical rubber membrane to the pedestal and securing with O-rings, a split mold was used, vacuum was supplied and upper section of membrane was secured. Similar to wet tamping method, specimen was compacted using a wooden rod until the desired relative density was obtained. A certain amount of confining pressure was applied to obtain a self-standing specimen. Percolating carbon dioxide and de-aired water through the specimen, Saturation was ensured by application of back pressure. Degree of saturation was controlled utilizing Skempton's pore water pressure parameter (B), which is desired to be greater than 0.96. Cell pressure is increased to obtain the required consolidation stress, and specimen is allowed to consolidate. In the next phase, undrained cyclic loading of

a predefined CSR was employed, and it is questioned if the specimens liquefied up to 20 cycles or not, or double amplitude axial strain exceeds 5%. During application of dynamic loading, excess pore water pressure, cyclic axial strain and cyclic deviator stresses were measured. Drainage valves were opened to record volume change in specimen. A series of tests were conducted by increasing the amplitude of cyclic load gradually.

2.3. Data in Brief

As mentioned above, the data set used in this study was obtained from a series cyclic triaxial tests performed on non-plastic silt specimens (Karakan et al., 2019a, b).Relative densities of specimens ranged between 30-80%. As a result of these experiments, it is determined whether these specimens were liquefied or not, and post-liquefaction of specimens were determined. The data set was created by using relative density (Dr), cyclic stress ratio (CSR), number of loading cycles (NoC) as inputs and pore water pressure (PWPR), cyclic axial strain (CAS), volumetric strain (VS) and factor of safety (FoS) as outputs.

In the first phase of this study, two different data sets were used by using the combinations of *CSR* with *NoC*. Data set was analysed using unsupervised clustering algorithms to classify these specimens as liquefied and nonliquefied. Later, an attempt was made to classify the post-liquefaction volumetric strains into three classes, based on and *CSR, NoC, PWPR, CAS*. In the second phase, the ability of ANFIS for estimation of post-liquefaction volumetric strains and factor of safety was questioned.

2.4. Unsupervised clustering algorithms

Data clustering is a discretization process which separates the elements or data points to be completely different according to their similarity. This similarity (or dissimilarity) criterion can be determined with the Euclidean distance for two data points as given in Eq. (1).

$$d(x,y)=\left(\sum_{j=1}^{d}(x_j - y_j)^2\right)^{1/2} \qquad (1)$$

Clustering can be divided into two groups as hard clustering and fuzzy clustering. In hard clustering, each element belongs only in one set and each set has at least an element (Gan et al., 2007). In fuzzy clustering, each element has a membership degree. Therefore, a data point with a partial membership can be element of more than one set (Ross, 2010).

2.4.1. Hard k-means clustering

K-means clustering is a method that provides a significant and interpretable clustering of a large number of data (McQueen, 1967). Algorithmically, clustering performed by use of a partition matrix, U (Eq. 2) and characteristic function, χ (Eq. 3). Euclidean distance is used to determine similarity or dissimilarity. Let *n* x *m* dimensional "*x*" data matrix will be divided into *c* clusters, where *k* and *i* is defined from 1 to *n* and *c*, respectively:

$$U = \{\chi_1, \chi_2, \chi_3, \dots, \chi_i\} \qquad (2)$$

$$\chi_i(x_k) = \begin{cases} 1, x_k \in i^{th} \ cluster \\ 0, x_k \notin i^{th} \ cluster \end{cases} \qquad (3)$$

If Equation (1) is arranged considering the data set, the Euclidean distance can be calculated by use of Equation (4).

$$d_{ik} = d(x_k - v_i) = \|x_k - v_i\|$$
$$= \sqrt{\sum_{j=1}^{m}(x_{kj} - v_{ij})^2} \qquad (4)$$

The vector of cluster centers (v_i) of the ith set is as in Equation (5):

$$v_i = \{v_{i1}, v_{i2}, v_{i3}, \ldots, v_{im}\} \qquad (5)$$

Cluster centers can be obtained as:

$$v_{ij} = \frac{\sum_{k=1}^{n} x_{ik} x_{kj}}{\sum_{k=1}^{n} x_{ik}} \qquad (6)$$

The objective function, J determines the most reasonable one between possible partitions (Eq. 7).

$$J(U, v) = \sum_{k=1}^{n} \sum_{i=1}^{c} x_{ik}(d_{ik})^2 \qquad (7)$$

Optimum partition matrix (U^*) and optimum cluster centers (v^*) are obtained by minimization of objective function (Eq. 8):

$$J(U^*, v^*) = \min\left[\sum_{k=1}^{n} \sum_{i=1}^{c} x_{ik}(d_{ik})^2\right] \qquad (8)$$

As a result of an iterative procedure, an objective function satisfying a stopping criterion is minimized. Partition matrix can be recalculated by updating characteristic function where r is iteration step and c is the number of clusters for all i and k (Ross, 2010):

$$x_{ik}^{(r+1)} = \begin{cases} 1, & d_{ik}^{(r)} = \min\left\{d_{jk}^{(r)}\right\} for\ all\ j \in c; \\ 0, & otherwise \end{cases} \qquad (9)$$

2.4.2. Fuzzy c-means algorithm

Fuzzy c-means method was first instructed by Bezdek (1981) and combines the advantages of fuzzification with hard k-means method (Ross, 2010). It was stated that, hard c-partition was also obtained while fuzzy clustering algorithms. Utilizing the membership degrees of fuzzy models, the concept of clustering was improved. Different from crisp clustering, a weighting parameter was included in the algorithm (Bezdek, 1981). Therefore, each data point can have a membership in more than one set due to partial membership (Ross, 2010). Accordingly, membership values can range between 0 to 1 in fuzzy clustering while this parameter can only take values of 0 or 1 in hard clustering. As in hard clustering, in order to classify a data set with n elements into c clusters, optimum partition matrix and optimum cluster centers could be determined by using minimized objective function (J) in Eq (10):

$$J_m(U^*, v^*) = \min\left[\sum_{k=1}^{n} \sum_{i=1}^{c} (\mu_{ik})^{m'}(d_{ik})^2\right] \qquad (10)$$

where U^* is the optimized partition matrix, v^* is the optimized vector of cluster centers, μ^{ik} is membership value for k^{th} data point in ith data set, m' is weighting parameter ranging between $[1, \infty)$, d_{ik} is Euclidean distance of kth data point in i^{th} data set (which is calculated by using Eq. 4 (Bezdek, 1981; Ross, 2010). The matrix of cluster centers, v can be calculated using following equation

$$v_{ij} = \frac{\sum_{k=1}^{n}(\mu_{ik})^{m'}\chi_{kj}}{\sum_{k=1}^{n}(\mu_{ik})^{m'}} \qquad (11)$$

for i = 1 to c and j = 1 to m

Fuzzy partitioning is completed when the optimized membership matrix is obtained by minimizing the objective function, where r is iteration step (Eq. 12).

$$\mu_{ik}^{(r+1)} = 1 \bigg/ \left[\sum_{j=1}^{c}\left(\frac{d_{ik}(r)}{d_{jk}(r)}\right)^{\frac{2}{m'-1}}\right] \qquad (12)$$

At the end of iterative approach, the sum of membership degree values for a set should be equal to 1, as shown in Equation 13:

$$\sum_{i \in I_k}\mu_{ik} = 1 \qquad (13)$$

For the termination of iterative process, the criterion of error tolerance should be satisfied, which minimizes the objective function, J (Eq. 14)

$$\left\|U^{(r+1)} - U^{(r)}\right\| \le \varepsilon \;(tolerance\;level) \qquad (14)$$

2.4.3. Self-organizing map (SOM)

Fuzzy c-means method was first instructed by Bezdek (1981) and combines the advantages of fuzzification with hard k-means method

Self-organizing map (SOM) is an artificial neural network that can be used in many areas - such as process analysis, machine perception, control and communication- and generally used for abstraction of data and then visualization by transferring it on a two dimensional map (Haykin, 1999; Kohonen, 2001). Current model widely used model was introduced by Kohonen. Success of Kohonen model is based on reduction in dimensions and "winner takes all" criterion (Haykin, 1999).

SOM architecture consists of an input layer which includes neurons fully connected to an output layer. Inner product with synaptic weight w is calculated for each input pattern x. Maximum value of inner product stands for minimization of lateral distance between x and w vectors, (Kohonen, 1996; Haykin, 1999; Gan et al., 2007). The distance (d) can be calculated by using Euclidean distance as in Eq. (15) where d is distance vector, x is input vector and w is synaptic weight matrix in network.

$$d_j = \left\|x_j - w_{ij}\right\| \qquad (15)$$

A discriminant function inducing competition between the neurons is found by neurons in the competitive layer. The winner in the com-

petition is simply the weight vector that approximates the input vector in the Euclidean distance.

In the second phase (cooperation) winning neuron determines the position of induced neurons for topological neighborhood (h_{ij}). Topological neighborhood can be obtained by using Gaussian function (Eq. 16) where σ is neighborhood width.

$$h_{ij} = e^{\left(\frac{d_{ij}^2}{2\sigma^2}\right)} \tag{16}$$

Lastly, in adaptation phase synaptic weights of neighborhood neurons are determined by using winning neuron and topological neighborhood (Eq. 17).

$$w_{ij}(t+1) = w_{ij}(t) + \eta(t)h_{ij}(t)\left[x_j(t) - w_{ij}(t)\right] \tag{17}$$

in which, t is iteration step, η is learning-rate parameter. Similar to all unsupervised clustering algorithms, SOM algorithm is an iterative procedure. The iteration continues until the winning neurons approximates to a constant (Kohonen, 2001; Haykin,1999).

2.4.4. Adaptive neuro-fuzzy inference system

Adaptive neural network is an artificial network algorithm consisting of nodes as processing units and links as direct connections between nodes. The definition "adaptive" stands for node outputs depending on modifiable parameters; thus, network can update itself, while the term "learning ability" refers to the parameters providing in a way that minimize error energy. Minimizing errors correspond to minimize the difference between desired outputs and actual outputs of network. Links of adaptive network are two types as feed forward and recurrent (Jang et al., 1997).

Fuzzy inference system (FIS) is a system that evaluates the inputs by considering membership functions with fuzzy rules and provides reasonable outputs. FIS has many optional models for use in various types of applications. The first of the three frequently used models is Mamdani model which was based on linguistic control rules and based on human experiences. Sugeno Model (also known as Takagi-Sugeno-Kang, TSK fuzzy model) created for more systematic fuzzy rules for input-output data sets. A third one is Tsukamoto model, which is less common compared to others (Jang et al., 1997). Jang (1993) suggested an effective inference system by using learning ability and update function for minimizing error of adaptive neurons and also membership function of fuzzy system. Thus, ANFIS is a combination of feed forward networks and Sugeno type FIS model. Typical rule set, which is based on Takagi and Sugeno's (1985) for Sugeno model was stated as Eq. (18) and Eq. (19). A five layered ANFIS architecture was demonstrated in Figure 2.

Rule 1.
If x is A_1 and y is B_1, then $f=p_1x+q_1y+r_1$ (18)

Rule 2.
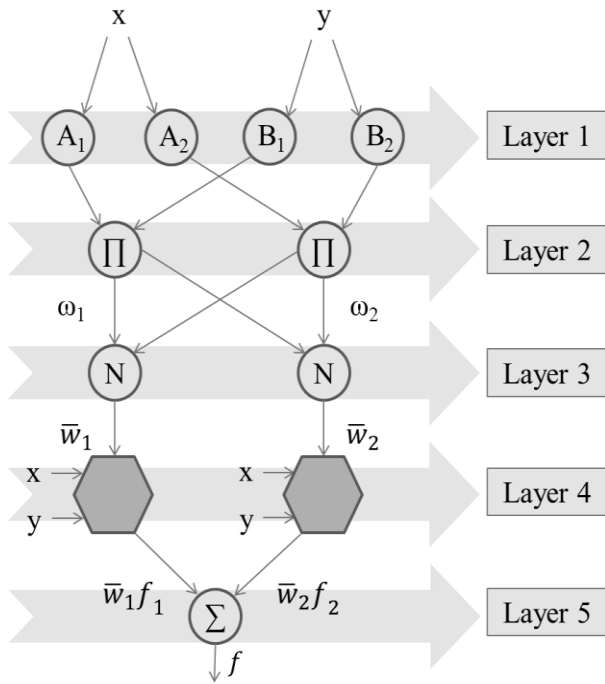I If x is A_2 and y is B_2, then $f=p_2x+q_2y+r_2$ (19)

Figure 2. ANFIS structure

In the first layer, outputs (also membership degrees) of each adaptive i node is calculated as in Equation (20) in which, x and y is inputs of i node, A_i or B_{i-2} is fuzzy sets of nodes:

$$O_{1,i} = \mu_{A_i}(x), \quad \text{for i} = 1,2 \quad \text{or} \tag{20}$$

$$O_{1,i} = \mu_{B_{i-2}}(y), \quad \text{for i} = 3,4$$

A membership function for A_i set is determined by using Gaussian function in Equation (21) where $\{a_i, b_i, c_i\}$ as parameter set.

$$\mu_{A_I(x)} = \left[1 + \left|\frac{x - c_i}{a_i}\right|^{2bi}\right]^{-1} \tag{21}$$

In the second layer each node is fixed and output of nodes refers to firing strength of the rule as a product of total incoming signals (Eq. 22).

$$O_{2,i} = w_i = \mu_{A_i}(x) \times \mu_{B_i}(y) \tag{22}$$

In the third layer, normalized firing strengths for each node is calculated via following equation:

$$O_{3,i} = \overline{w}_i = {w_i}/{(w_1 + w_2)}, i = 1,2. \tag{23}$$

The effect i^{th} rule on normalized firing strength and output is in fourth layer (Eq. 24)

$$O_{4,i} = \overline{w}_i f_i = \overline{w}_i(p_i x + q_i y + r_i) \tag{24}$$

in which, p, q and r (also known as consequent parameters) are parameter set of ith node. All incoming signals are collected in one node in fifth layer. The total output (ANFIS output) can be calculated by Equation 25 (Jang, 1993; Jang et al., 1997).

$$O_{5,i} = \sum \overline{w}_i f_i = \overline{w}_1 f_1 + \overline{w}_2 f_2 \tag{25}$$

for i=1,2

It should be noted that, further information about models can be found in literature (Sezer et al., 2007, 2010)

3. Results and Discussion

A nonplastic silt was subjected to liquefaction testing and the test results were published previously (Tanrinian; 2017; Karakan et al., 2019a, b). Therefore, it was aimed to classify the data in terms of liquefaction susceptibility and post-liquefaction volumetric strain. As mentioned previously, data including relative density (%), cell & back pressure (kPa), consolidation pressure (kPa), cyclic stress ratio, number of cycles, pore water pressure ratio (%), volumetric strain (%), cyclic axial strain (%), double amplitude axial strain (%), shear strain (%), post liquefaction volumetric strain (%), factor of safety as well as liquefaction state were tabulated for a better evaluation of test results. Parameters affecting liquefaction are selectively subjected to clustering and ANFIS analyses. It was aimed to estimate / verify the liquefaction potential, post-liquefaction volumetric strains and factor of safety by use of parameters obtained before and during testing.

3.1. Statistical analysis of test results

Several efforts using unsupervised clustering algorithms and ANFIS were made to estimate the liquefaction state / post liquefaction volumetric strain and factor of Safety obtained from results cyclic triaxial test on a nonplastic silts. This test is time consuming and needs a sophisticated approach to obtain the liquefaction characteristics of a certain soil. Besides, several complications during testing may affect the test results, and verification of results obtained may be necessary.

The statistical analysis and frequency histograms of input and output parameters were given in Table 1 and Figure 3, respectively.

There is only one peak in the frequency histograms, except that the PWPR histogram has two peaks. Therefore, it was understood that the frequency diagram of CSR, NoC, CAS, PLVS and FoS fit normal distribution curve better when compared to PWPR. Analyzing the PWPR, CAS, PLVS and FoS values in Table 1, it is understood that these parameters have a comparably high standard deviation, in comparison with the average value. All parameters in Table 1 but NoC are right skewed. Kurtosis coefficients of the variables (Except FoS) are less than zero, indicating that peaked nesses of the distributions are smaller in comparison with gauss distribution curve. Histograms of dependent parameters in Figure 2 come up with the possibility of classification of inputs, unsupervised clustering and ANFIS methods are applicable to data in hand

3.2. Leveraging soft computing methods for estimation of liquefaction susceptibility and post-liquefaction behavior

3.2.1. Classification of liquefied / nonliquified silts using NoC and CSR

As an initial approach, it is known that number of cycles (NoC) and cyclic stress ratio (CSR) are known to influence liquefaction test results. Therefore, a two parameter classification trials were made using these parameters. As shown in Figure 3, NoC-CSR plot showed a clear clustered behaviour, and since majority of nonliquified specimens are close to NoC=20, it was evident that this classification was successful. It should be noted that, CSR=0.1 is an identifier of liquefaction susceptibility, only three of specimens beyond this value did not liquefy. It should be emphasized that, due to clear distinction between two datasets, performances of clustering algorithms were equivalent (Table 2).
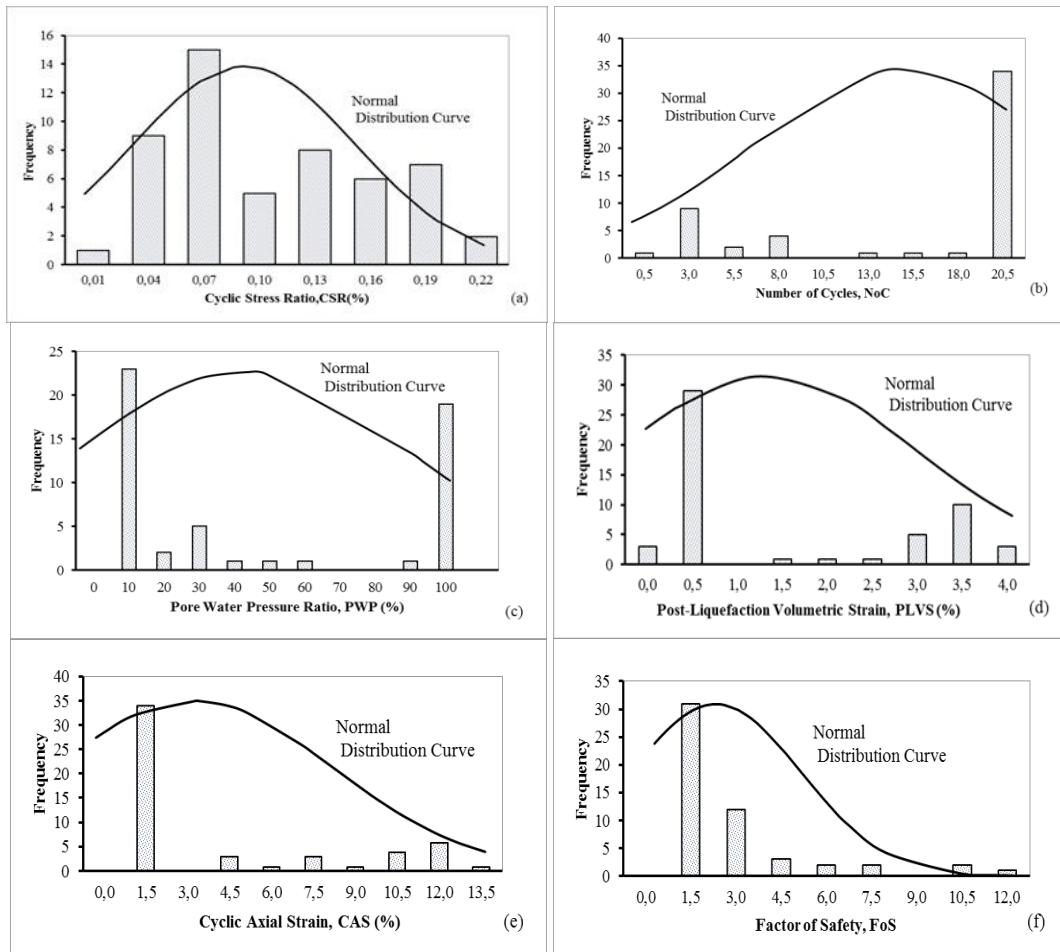
Figure 3. Frequency histograms for a) CSR b) NoC c) PWP d) PLVS e) CAS f) FoS

Table 1. Descriptive statistics of input and output data

Parameter	CSR	NoC	PWP (%)	CAS (%)	PLVS (%)	FoS
Mean	0.09	14.66	44.48	3.20	1.20	2.23
Standard Error	0.20	1.74	9.60	12.80	5.29	2.29
Median	0.09	20.00	21.03	0.13	0.08	1.20
Standard Deviation	0.06	7.79	44.04	4.56	1.48	2.51
Variance	0.00	60.73	1939.12	20.81	2.18	6.30
Kurtosis	-0.96	-1.08	-1.79	-0.68	-1.64	4.57
Skewness	0.33	-0.90	0.39	1.01	0.56	2.23
Range	0.21	19.50	99.01	12.73	3.63	10.58
Min	0.01	0.50	0.99	0.01	0.00	0.41
Max	0.22	20.00	100.00	12.73	3.63	10.99

The relationship among NoC and CSR obtained from tests performed on liquefied and nonliquefied silts (Figure 4) are in agreement with those obtained from unsupervised clustering algorithms. Experiments with CSR<0.1 ended up without liquefaction, and results of HKM, FCM and SOM algorithm is in line with experimental outcomes. On the contrary, it was observed that all the tests with CSR>0.14 liquefied, which were also successfully modelled by results of unsupervised clustering analyses. Analysing Table 2, it is clear that the cluster centres were very close to each other, and the classification rates were same. Overall performances of the algorithms were similar, and above-mentioned parameters could be used for estimation / verification of liquefaction susceptibility of nonplastic silts.
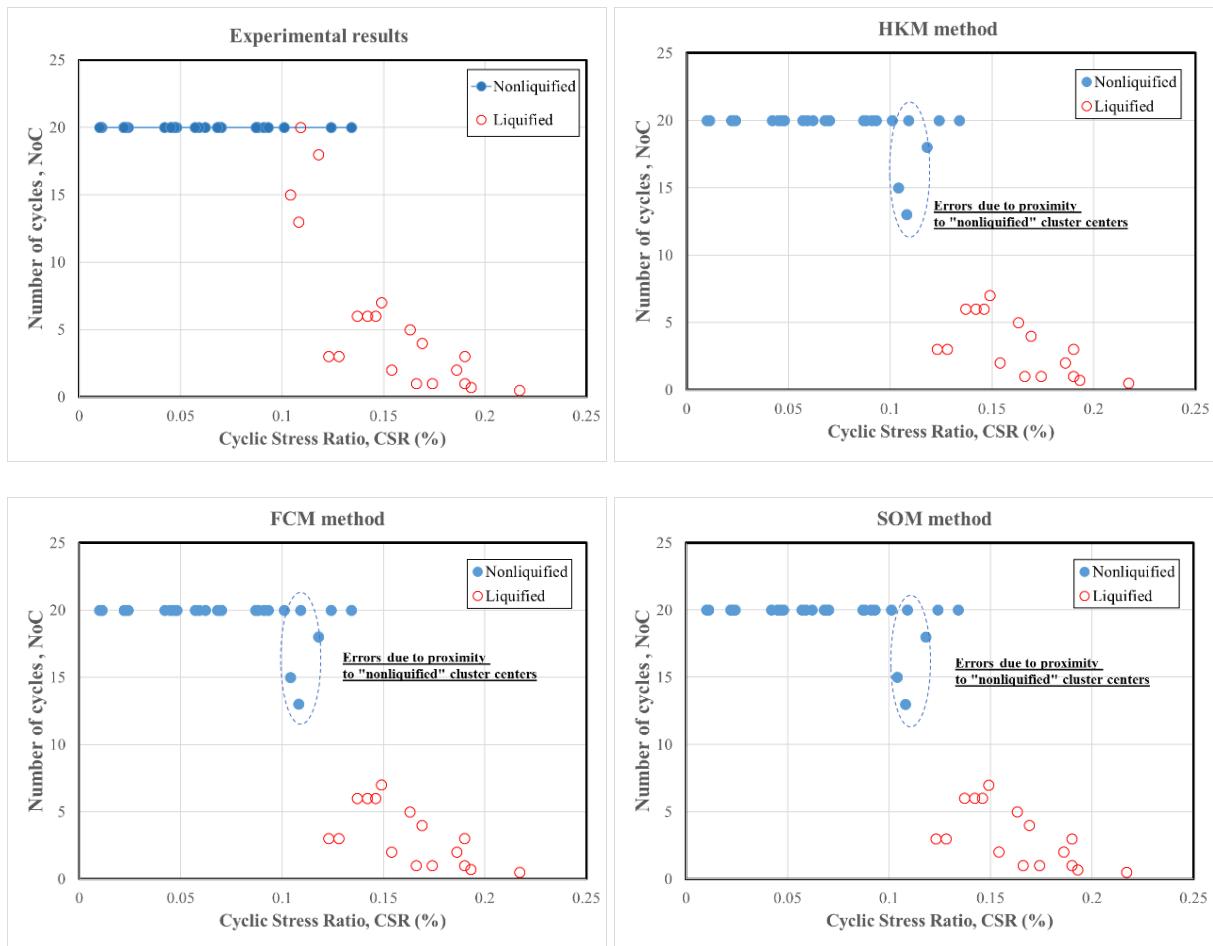

Figure 4. Classification of liquefied / nonliquefied specimens using CSR and NoC:
a) Experimental results b) HKM c) FCM d) SOM approach

Table 2. Liquefaction susceptibility classified using CSR and NoC. Misclassification rates and overall success were also tabulated.

Parameter	CSR	NoC	PWP (%)	CAS (%)	PLVS (%)	FoS
Mean	0.09	14.66	44.48	3.20	1.20	2.23
Standard Error	0.20	1.74	9.60	12.80	5.29	2.29
Median	0.09	20.00	21.03	0.13	0.08	1.20
Standard Deviation	0.06	7.79	44.04	4.56	1.48	2.51
Variance	0.00	60.73	1939.12	20.81	2.18	6.30
Kurtosis	-0.96	-1.08	-1.79	-0.68	-1.64	4.57
Skewness	0.33	-0.90	0.39	1.01	0.56	2.23
Range	0.21	19.50	99.01	12.73	3.63	10.58
Min	0.01	0.50	0.99	0.01	0.00	0.41
Max	0.22	20.00	100.00	12.73	3.63	10.99

3.2.2. Classification of volumetric strains using CSR, NoC, PWPR and AS

In the second phase, a 4-parameter input was decided to assess whether we can estimate the level of post-liquefaction volumetric strains (PLVS). In this manner, cyclic stress ratio (CSR), number of cycles (NoC), pore water pressure ratio (PWPR) and cyclic axial strain (CAS) were determined as inputs to clustering scheme. In this regard, three clusters are selected, or the experimental PLVS values are divided into three categories as low (<1%), medium (≥1% and ≤ 2%) and large (>2%). Experimental errors or failure in experiments may cause misleading results, therefore, this classification effort could also be used for verification of experimental results, as well as estimation of level of volumetric strains by under certain experimental conditions is possible.

Using these four parameters, clustering analyses were performed to estimate the level of PLVS. The results are presented in Figure 5. It is evident that, the data points are clustered distinctly, and the post-liquefaction volumetric strains are classified, according to the limits proposed. It should be noted that, apart from those shown in Figures, number of cycles are also included in the analyses. Performances of the algorithms are satisfactory, it is interesting to note there that, although FCM is a better classifier in comparison with HKM thanks to fuzzification ability, interfering classes (proximity of data in distinct classes) increased the success of HKM. Same is valid for SOM, although it is expected that performances of FCM and SOM algorithms would be better than that of HKM, a reverse behaviour is observed. The data points in blue circles in Figure 5 are misclassified, and these two classifiers are less capable of distinguish among PVLS<1 and 1<=PVLS<=2. This could also be observed from cluster centers, center coordinates of HKM are somewhat different from those of FCM and SOM.
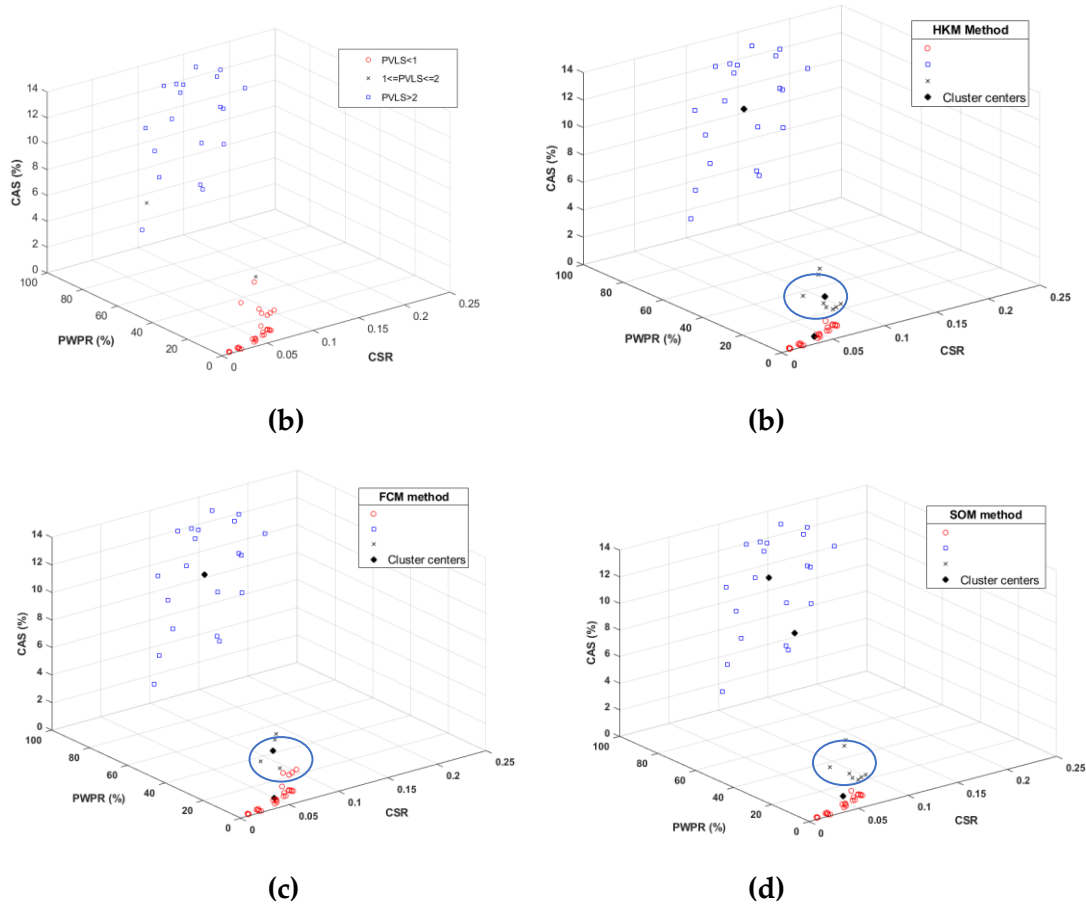
Figure 5. Clustering PLVS by CSR, NoC, PWPR and CAS a) Experimental data b) HKM c) FCM d) SOM methods. Black diamonds are cluster centers (actually, there is one more dimension, which cannot be represented here). Data points in blue circle are misclassified.

Analyzing the partial membership values in Figure 6, it is understood that increased shared membership values of a data points somehow hindered its correct classification. In other words, power of classification method adversely affected on performance of the classifier, data points comprised by a different cluster is effective on misclassification rates.

3.2.3. Classification of volumetric strains using CSR, NoC, PWPR and AS

In the second phase, a 4-parameter input was decided to assess whether we can estimate the level of post-liquefaction volumetric strains (PLVS). In this manner, cyclic stress ratio (CSR), number of cycles (NoC), pore water pressure ratio (PWPR) and cyclic axial strain (CAS) were determined as inputs to clustering
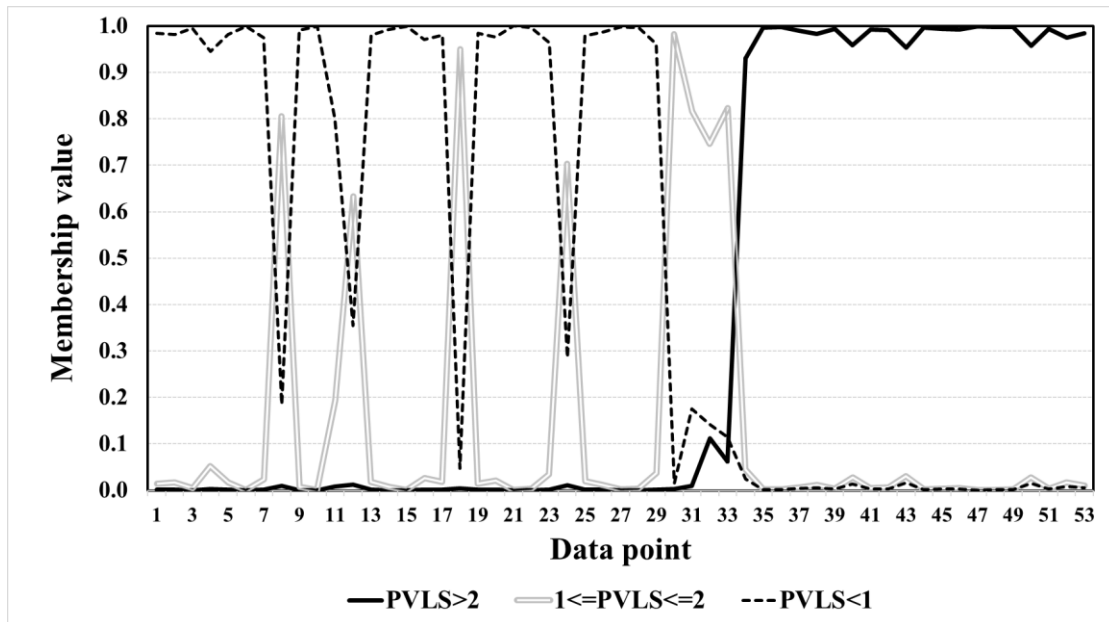
Figure 6. Membership values of three PLVS classes

scheme. In this regard, three clusters are selected, or the experimental PLVS values are divided into three categories as low (<1%), medium (≥1% and ≤ 2%) and large (>2%) (Table 3). Experimental errors or failure in experiments may cause misleading results, therefore, this classification effort could also be used for verification of experimental results, as well as estimation of level of volumetric strains by under certain experimental conditions is possible.

Using these four parameters, clustering analyses were performed to estimate the level of PLVS. The results are presented in Figure 5. It is evident that, the data points are clustered distinctly, and the post-liquefaction volumetric strains are classified, according to the limits proposed. It should be noted that, apart from those shown in Figures, number of cycles are also included in the analyses. Performances of

the algorithms are satisfactory, it is interesting to note there that, although FCM is a better classifier in comparison with HKM thanks to fuzzification ability, interfering classes (proximity of data in distinct classes) increased the success of HKM. Same is valid for SOM, although it is expected that performances of FCM and SOM algorithms would be better than that of HKM, a reverse behaviour is observed. The data points in blue circles in Figure 5 are misclassified, and these two classifiers are less capable of distinguish among PVLS<1 and 1<=PVLS<=2. This could also be observed from cluster centers, center coordinates of HKM are somewhat different from those of FCM and SOM

Analyzing the partial membership values in Figure 6, it is understood that increased shared membership values of a data points somehow

hindered its correct classification. In other words, power of classification method adversely affected on performance of the classifier, data points comprised by a different cluster is effective on misclassification rates

3.2.4. Attempts for estimation of factor of safety (FoS) and post liquefaction volumetric strain (PLVS) by use of ANFIS

The next phase consists of questioning the ability of adaptive neuro-fuzzy inference systems (ANFIS) in modelling in PLVS and FoS. Arbitrary selected inputs which may be useful in modelling ANFIS are used. In this regard, 70% and 30% of the dataset are randomly allocated for training and testing datasets, respectively.

A Sugeno-type fuzzy model and triangular input membership function (trimf) are employed in analyses. Twenty-six different models of two, three and four inputs were used to predict factor of safety. CSR, PWPR, Dr, CAS and NoC were used as inputs. Grid partitioning is used to construct fuzzy inference system.

For simplicity, Table 4 shows the input and output parameters, model numbers, and mean square error and coefficient of determination (R^2) values of models for training and testing data. The coefficient of determination is a measure of the goodness of fit, which is expressed as (Rayner et al., 2009).

Table 3. Post-liquefaction volumetric strains classified using CSR, NoC, PWPR and CAS. Misclassification rates and overall success were also tabulated.

	PARAMETER		HKM	FCM	SOM
Cluster centers	**CSR**	**PVLS<1**	0.049	0.042	0.044
		1<=PVLS<=2	0.109	0.099	0.101
		PVLS>2	0.153	0.154	0.160
	NoC	**PVLS<1**	20.000	20.000	20.000
		1<=PVLS<=2	20.000	19.994	20.000
		PVLS>2	5.860	5.727	4.894
	PWPR	**PVLS<1**	7.566	5.406	5.614
		1<=PVLS<=2	39.483	30.987	30.576
		PVLS>2	99.012	99.000	98.837
	CAS	**PVLS<1**	0.045	0.033	0.033
		1<=PVLS<=2	0.215	0.175	0.170
		PVLS>2	8.363	8.435	8.530
Misclassification		**PVLS<1**	0/19	7/19	7/19
		1<=PVLS<=2	1/2	1/2	1/2
		PVLS>2	3/32	0/32	0/32
Overall success (%)			92.5	84.9	84.9

Table 4. Summary of ANFIS analyses for prediction of PLVS and FoS.

Dr	CSR	NoC	PWPR	CAS	Model No. (Output PLVS)	Training MSE	Training R²	Testing MSE	Testing R²	Model No. (Output FoS)	Training MSE	Training R²	Testing MSE	Testing R²
+	+	+	+	+	1	0.000	1.000	1.846	0.077	27	0.116	0.984	332.0	0.011
	+	+	+	+	2	0.026	0.988	1.287	0.356	28	0.213	0.971	325.0	0.009
+		+	+	+	3	0.006	0.997	0.834	0.583	29	1.835	0.751	392.2	0.096
+	+	+		+	4	0.000	1.000	0.286	0.857	30	0.107	0.986	28.28	0.002
+	+	+	+		5	0.000	1.000	1.062	0.469	31	0.050	0.993	5.374	0.132
+	+	+			6	0.000	1.000	0.178	0.911	32	0.168	0.977	75.76	0.069
+	+		+		7	0.042	0.980	1.545	0.227	33	0.284	0.961	16.83	0.000
+	+			+	8	0.002	0.999	1.000	0.500	34	0.167	0.977	2.727	0.367
+		+	+		9	0.000	1.000	0.532	0.734	35	0.049	0.993	8.868	0.000
+		+		+	10	0.009	0.996	1.509	0.245	36	1.974	0.732	36.82	0.048
+			+	+	11	0.007	0.996	1.607	0.196	37	3.685	0.500	3.955	0.128
	+	+	+		12	0.025	0.988	0.208	0.896	38	1.811	0.754	88.99	0.049
	+	+		+	13	0.028	0.987	0.061	0.969	39	0.369	0.950	0.105	0.029
	+		+	+	14	0.026	0.988	1.160	0.420	40	0.268	0.964	21.40	0.028
		+	+	+	15	0.042	0.980	1.036	0.482	41	0.218	0.970	12.44	0.379
+	+				16	0.029	0.986	0.096	0.952	42	1.457	0.802	1.059	0.002
+		+			17	0.005	0.998	1.150	0.425	43	0.181	0.975	5.304	0.123
+			+		18	0.081	0.961	0.454	0.773	44	5.149	0.301	8.189	0.244
+				+	19	0.013	0.994	0.174	0.913	45	2.003	0.728	3.954	0.056
+					20	0.011	0.995	0.305	0.847	46	4.120	0.441	10.66	0.175
	+	+			21	0.093	0.956	0.718	0.641	47	0.479	0.935	21.00	0.046
	+		+		22	0.044	0.979	0.902	0.549	48	0.367	0.950	3.323	0.010
	+			+	23	0.022	0.989	0.511	0.745	49	0.275	0.963	11.66	0.001
		+	+		24	0.030	0.985	0.166	0.917	50	1.839	0.750	2.779	0.105
		+		+	25	0.029	0.986	0.740	0.630	51	3.392	0.540	3.562	0.040
			+	+	26	0.052	0.975	0.129	0.935	52	1.745	0.763	89.32	0.036

$$R^2 = 1 - \frac{\sum\limits_{i=1}^{n} (y_i - p_i)^2}{\sum\limits_{i=1}^{n} \left[y_i - \frac{1}{n} \sum\limits_{i=1}^{n} y_i \right]^2} \qquad (26)$$

where yi and pi are real values and estimates and n is number of data. On the other hand, the mean squared error (MSE) measures the average of the squares of the errors or difference between the estimated and the actual values (Sammut and Webb, 2011).

$$RMSE = \frac{\sum\limits_{i=1}^{n} (y_i - p_i)^2}{n} \qquad (27)$$

A total of 52 models were established on an elimination basis, and the performance of the models were comparatively investigated. It should be emphasized that, output of half of the models is PLVS, and output of the rest is FoS. At first sight, it is evident that PLVS can be modelled using inputs, however the same interpretation cannot be made for FoS. Despite the relatively high values in training phase, at testing phase, the models established for FoS concluded unacceptably high MSE and low R^2 values. Highest R^2 value was obtained from Model 41, using NoC, PWPR and CAS as inputs. Since these parameters are obtained during testing, use of this "best of the best" model is not advised due to high mean square errors and low performance estimates of factor of safety. A maximum R^2 value of 0.379 gives

clues for estimation trials: The five inputs, obtained at the beginning of the test and during testing is incapable of estimating the factor of safety at an acceptable level.

Coming back to PLVS, results are more promising. After training phase, R^2 of 26 of models are greater than 0.97, and in testing phase, R^2 of many models are greater than 0.90, accompanied by extremely low MSE values. Although very R^2 models can be obtained by use of 5 and 3 parameter models (model 1 and 2 concluded R^2 values of 0.077 and 0.196 as well as high MSE values), it is understood that these parameters have a potential in prediction of PLVS. Model 13, with R^2 and MSE values of 0.969 and 0.061 on testing data showed the best performance, and Models 6, 16, 19, 24 and 26 have potential in PLVS prediction. These models have different input combinations; however, it is clear that cyclic axial strain has an influence on prediction capability. It should be emphasized that, predictions can be made with parameters that can be determined before testing (Model 16-Dr and CSR). Performances of best ANFIS models are also summarized with the results given in Figure 7, which shows the scatter plots of the estimated and actual values of PLVS and FoS. It is observed that, training phase works almost perfect. The data is scattered in the vicinity of line of equality (predicted values=actual values). The plot pf PLVS estimates in testing phase is also close to line of equality, however, same interpretation cannot be made for FoS, even though results of the best model (Model 34) is shown here.
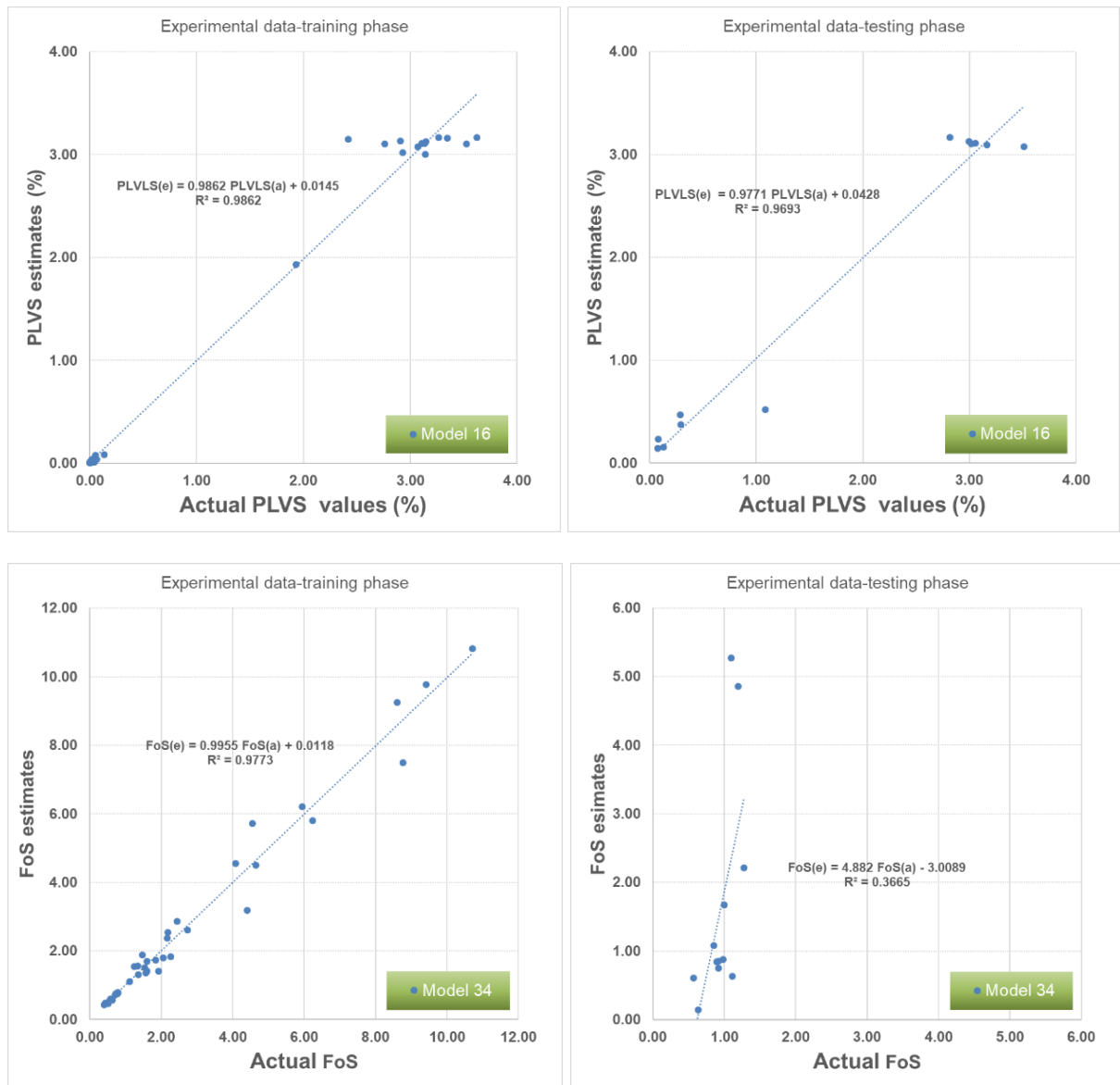
Figure 7. Scatterplots for estimates of PLVS and FoS in training and testing phases: a) PLVS-training, b) PLVS-testing, c) FoS -training, d) FoS-testing

4.   Conclusions

This study presents modelling attempts for classification/estimation/verification of liquefaction susceptibility, postliquefaction volumetric strains and factor of safety. In this scope, results obtained from experiments were classified using HKM, FCM and SOM algorithms. Using a trial-and error approach, the cyclic stress ratio and number of cycles to liquefaction are used to classify liquefaction

state. The results revealed that, liquefaction is observed by testing specimens at a CSR less than 0.1. On the contrary, another interesting outcome, specimens tested under CSR greater than 0.14 liquefied irrespective of the initial relative density of specimen. The liquefaction states obtained by clustering algorithms are in accordance with experimental outcomes, which proves that the two parameters determined before testing is capable of estimating if a specimen will liquefy or not. This information can also be used for verification purposes. These clustering methods are also employed to classify post-liquefaction volumetric strains (PLVS) in three classes: PLVS<1, 1≤ PLVS ≤2 and PLVS>2. It is evident that, while maximum pore water pressure ratio (PWPR) obtained by testing specimens at a CSR level smaller than 0.1 is 40%, corresponding values obtained from HKM, FCM and SOM methods are 20%, 25% and 15%, respectively. Corresponding PLVS values are found to be less than 0.1. Experimental CAS values are in agreement with those obtained by the classifiers, for PLVS>2 these values range among 4% and 14%.

In the second phase of the study, 52 ANFIS models were employed to model the PLVS and factor of safety against liquefaction (FoS). In this regard, the data is divided into training and testing data on a random basis (70% to 30% respectively), and twenty-six different models of two, three and four inputs were used to predict factor of safety. In this scope, combinations of cyclic stress ratio, pore water pressure ratio, initial relative density, cyclic axial strain and number of cycles were used as inputs. At training phase, the mapping between model outcomes and actual values is scattered in the vicinity of line of equality. Results show that ANFIS, use of these inputs is only capable of determination of PLVS, however, FoS estimation of above mentioned models are far from being accurate.

It is understood that the liquefaction state and post liquefaction volumetric strain can be estimated by use of soft computing methods. On the other hand, there is also a potential of verification of results of ambiguous test data. It is advised to carry out additional tests on different types of nonplastic silts, for verification of the results obtained.

References

Aidona, E., Grison, H., Petroanvsky, E. et al. (2016). Magnetic characteristics and trace elements concentration in soils from Anthemountas River basin (North Greece): discrimination of different sources of magnetic enhancement. Environ Earth Sci 75, 1375. https://doi.org/10.1007/s12665-016-6114-3

Andrus, R. D., & Stokoe II, K. H. (2000). Liquefaction resistance of soils from shear-wave velocity. Journal of geotechnical and geoenvironmental engineering, 126(11), 1015-1025.

ASTM D4253-16, Standard test methods for maximum index density and unit weight of soils using a vibratory table, ASTM International, West Conshohocken, PA, 2016a, www.astm.org.

ASTM D4254-16, Standard Test Methods for Minimum Index Density and Unit Weight of Soils and Calculation of Relative Density, ASTM International, West Conshohocken, PA, 2016b, www.astm.org

Bezdek JC. (1981). Pattern recognition with fuzzy objective function algorithms. New York: Plenum.

Boulanger RW. (2003). High overburden stress effects in liquefaction analyses. J. GeotechGeoenviron. 129, pp.1071–82.

Boulanger, R. W., & Idriss, I. M. (2014). CPT and SPT based liquefaction triggering procedures. Report No. UCD/CGM.-14, 1.

Carraro, JAH, Bandini, P, Salgado, R. (2003). Liquefaction resistance of clean and nonplastic silty sands based on cone penetration resistance. J. Geotech. Geoenviron. 129:965–76.

Chen, YC, and Liao, TS. (1999). Studies of the state parameter and liquefaction resistance of sand. In: Proceedings of the 2nd international conference on earthquake geotechnical engineering, Lisbon Portugal. p. 513–518.

Dobry, R., Ladd, R. S., Yokel, F. Y., Chung, R. M., & Powell, D. (1982). Prediction of pore water pressure buildup and liquefaction of sands during earthquakes by the cyclic strain method (Vol. 138). Gaithersburg, MD: National Bureau of Standards.

Fattahi, H. (2016). Indirect estimation of deformation modulus of an in situ rock mass: an ANFIS model based on grid partitioning, fuzzy c-means clustering and subtractive clustering. Geosciences Journal, 20(5), 681-690.

Gan, G., Ma, C., & Wu, J. (2007). Data clustering: theory, algorithms, and applications. Society for Industrial and Applied Mathematics.

Gokceoglu, C. A. N. D. A. N., Sonmez, H., & Kayabasi, A. (2003). Predicting the deformation moduli of rock masses. International Journal of Rock Mechanics and Mining Sciences, 40(5), 701-710.

Goktepe, A. B. , İnan Sezer, G., Sezer, A., & Ramyar, K., (2007). Determination of sulfate resistance level of cements using unsupervised clustering algorithms. Cement And Concrete World, vol.12, 44-55.

Goktepe, A. B., Altun, S., & Sezer, A. (2005). Soil clustering by fuzzy c-means algorithm. Advances in Engineering Software, 36(10), 691-698.

Hanesch, M., Scholger, R., & Dekkers, M. J. (2001). The application of fuzzy c-means cluster analysis and non-linear mapping to a soil data set for the detection of polluted sites. Physics and Chemistry of the Earth, Part A: Solid Earth and Geodesy, 26(11-12), 885-891.

Haykin, S., 1999. Neural Networks. Prentice-Hall, New Jersey, NY.

Hot E, Popović-Bugarin V (2016) "Soil data clustering by using K-means and fuzzy K-means algorithm", Telfor Journal, 8(1), 56-61.

Hyde AF, Higuchi T, Yasuhara K. (2007). Postcyclic recompression, stiffness, and consolidated cyclic strength of silt. J GeotechGeoenviron Eng. 133(4):416–23.

Idriss, I. M., & Boulanger, R. W. (2008). Soil liquefaction during earthquakes. Earthquake Engineering Research Institute.

Jang, J. S. (1993). ANFIS: adaptive-network-based fuzzy inference system. IEEE transactions on systems, man, and cybernetics, 23(3), 665-685.

Jang, J. S. R., Sun, C. T., &Mizutani, E. (1997). Neuro-fuzzy and soft computing-a computational approach to learning and machine intelligence [Book Review]. IEEE Transactions on automatic control, 42(10), 1482-1484.

JGS 0520-2000, 2000a. Preparation of soil specimens for triaxial tests. Japanese Geotechnical Society.

JGS 0541-2000, 2000b. Method for cyclic undrained triaxial tests on soils. Japanese Geotechnical Society.

Jokar, M. H., & Mirasi, S. (2018). Using adaptive neuro-fuzzy inference system for modelling unsaturated soils shear strength. Soft Computing, 22(13), 4493-4510.

Jurko, J, Sassa, K, Fukuoka, H. (2006). Dynamic behavior of gentle silty slopes based on undrained cyclic shear test. In:Marui Hideaki, editor. Disaster mitigation of debris flows, slope failure sand landslides. Tokyo, Japan: Universal Academy Press, Inc. pp.411–420.

Karakan, E., Sezer, A., & Tanrinian, N. (2019b). Evaluation of effect of limited pore water pressure development on cyclic behavior of a nonplastic silt. Soils and Foundations, 59(5), 1302-1312.

Karakan, E., Sezer, A., Tanrınian, N., & Altun, S. (2018b). Behavior of a dense nonplastic silt under cyclic loading. Anadolu Üniversitesi Bilim Ve Teknoloji Dergisi-B Teorik Bilimler, 6, 183-191.

Karakan, E., Tanrınian, N., & Sezer, A. (2018a). Evaluation of Excess Pore Water Pressure Build-up During Cyclic Triaxial Tests on a Nonplastic Silt. Düzce Üniversitesi Bilim ve Teknoloji Dergisi, 6(2), 513-524.

Karakan, E., Tanrinian, N., & Sezer, A. (2019a). Cyclic undrained behavior and post liquefaction settlement of a nonplastic silt. Soil Dynamics and Earthquake Engineering, 120, 214-227.

Kayadelen, C., Günaydın, O., Fener, M., Demir, A., & Özvan, A. (2009). Modelling of the angle of shearing resistance of soils using soft computing systems. Expert Systems with Applications, 36(9), 11814-11826.

Kayen, R. E., & Mitchell, J. K. (1997). Assessment of liquefaction potential during earthquakes by Arias intensity. Journal of Geotechnical and Geoenvironmental Engineering, 123(12), 1162-1174.

Kenny TC. (1977). Residual strength of mineral textures. Proceedings of the 9th ICSMFE, Tokyo, vol. 1.; p. 155–60.

Kohonen T. (2001) Learning Vector Quantization. In: Self-Organizing Maps. Springer Series in Information Sciences, vol 30. Springer, Berlin, Heidelberg

Kohonen, T., Oja, E., Simula, O., Visa, A., &Kangas, J. (1996). Engineering applications of the self-organizing map. Proceedings of the IEEE, 84(10), 1358-1384.

Liu, L., Moayedi, H., Rashid, A. S. A., Rahman, S. S. A., & Nguyen, H. (2020). Optimizing an ANN model with genetic algorithm (GA) pre-

dicting load-settlement behaviours of eco-friendly raft-pile foundation (ERP) system. Engineering with Computers, 36(1), 421-433.

Lu, L.; Liu, C.; Li, X.; Ran, Y. (2017). Mapping the Soil Texture in the Heihe River Basin Based on Fuzzy Logic and Data Fusion. Sustainability, 9, 1246.

McQueen, J. (1967). Some methods for classification and analysis of multivariate observations. In Proceedings of the fifth Berkeley symposium on mathematical statistics and probability (Vol. 1, No. 14, pp. 281-297).

Moayedi, H and Rezai A. 2020. The feasibility of PSO–ANFIS in estimating bearing capacity of strip foundations rested on cohesionless slope. Neural Computing and Applications, https://doi.org/10.1007/s00521-020-05231-9.

O'Reilly MP, Brown SF, Overy RF. (1991). Cyclic loading of silty clay with drainage periods. J Geotech Eng. 117(2):354–62.

Odhiambo, L. O., Freeland, R. S., Yoder, R. E., & Hines, J. W. (2004). Investigation of a fuzzy-neural network application in classification of soils using ground-penetrating radar imagery. Applied engineering in agriculture, 20(1), 109.

Papadopoulou, A., & Tika, T. (2008). The effect of fines on critical state and liquefaction resistance characteristics of non-plastic silty sands. Soils and foundations, 48(5), 713-725.

Polito, C. P., & Martin II, J. R. (2001). Effects of nonplastic fines on the liquefaction resistance of sands. Journal of Geotechnical and Geoenvironmental Engineering, 127(5), 408-415.

Provenzano P, Ferlisi S, Musso A. 2004. Interpretation of a model footing response through

an adaptive neural fuzzy inference system, Computers and Geotechnics, 31(3), 251-266.

Qadimi, A., & Mohammadi, A. (2014). Evaluation of state indices in predicting the cyclic and monotonic strength of sands with different fines contents. Soil Dynamics and Earthquake Engineering, 66, 443-458.

Rangel JS, Iturraran-Viveros U, Ayala AG, Cervantes F. 2005. Tunnel stability analysis during construction using a neuro-fuzzy system. International Journal for Numerical and Analytical Methods in Geomechanics, 29(15):1433 – 1456

Rayner, JCW., Thas O., Best, DJ. (2009) Smooth Tests of Goodness of Fit: Using R, 2nd edition, Wiley, 281 p.

Ross, T. J. (2010). Fuzzy logic with engineering applications (Vol. 3). New York: Wiley.

Sammut, G., Webb, GI. (2011) Encyclopedia of Machine Learning, Nwe York Springer Science and Business Media.

Seed, H. B., & Idriss, I. M. (1969). Influence of soil conditions on ground motions during earthquakes. Journal of the Soil Mechanics and Foundations Division, 95(1), 99-137.

Seed, H. B., & Idriss, I. M. (1971). Simplified procedure for evaluating soil liquefaction potential. Journal of Soil Mechanics & Foundations Div.

Seed, H.B, Tokimatsu, K., Harder, L. F., & Chung, R. M. (1985). Influence of SPT procedures in soil liquefaction resistance evaluations. Journal of geotechnical engineering, 111(12), 1425-1445.

Sezer A. 2013. Simple models for the estimation of shearing resistance angle of uniform sands, Neural Computing & Applications, 22(1), 111-123.

Sezer, A., Göktepe, A. B. , & Altun, S., (2007). Estimation of Maximum Dry Unit Weight of Soils via Artificial Neural Networks . International Symposium on Innovations in Intelligent Systems and Applications - INISTA 2007 (pp.225-229). İstanbul, Turkey

Sezer, A., Göktepe, B. A., & Altun, S. (2010). Adaptive neuro-fuzzy approach for sand permeability estimation. Environmental Engineering & Management Journal (EEMJ), 9(2).

Shi, M., Chen, J., Song, Y. et al. (2016). Assessing debris flow susceptibility in Heshigten Banner, Inner Mongolia, China, using principal component analysis and an improved fuzzy C-means algorithm. Bull EngGeol Environ 75, 909–922.
 https://doi.org/10.1007/s10064-015-0784-z

Song, S., Wang, Q., Chen, J. et al., (2017). Fuzzy C-means clustering analysis based on quantum particle swarm optimization algorithm for the grouping of rock discontinuity sets. KSCE J CivEng 21,1115–1122
https://doi.org/10.1007/s12205-016-1223-9

Sorensen, K. K., Baudet, B. A., & Simpson, B. (2007). Influence of structure on the time-dependent behaviour of a stiff sedimentary clay. Géotechnique, 57(1), 113-124.

Stamatopoulos CA, Balla L. (2004). Cyclic strength of sands in terms of the state parameter. In:Proceedings of the 11th international conference on soil dynamics and earthquake engineering (11th ICSD) and the third international conference on geotechnical earthquake engineering.

Stamatopoulos CA. (2010). An experimental study of the liquefaction strength of silty sands in terms of the state parameter. Soil Dyn. Earthq. Eng. 30 (Issue 8):662–78.

Takagi, T., & Sugeno, M. (1985). Fuzzy identification of systems and its applications to modelling and control. IEEE transactions on systems, man, and cybernetics, (1), 116-132.

Tanrınıan, N., Karakan, E., Sezer, A., & Altun, S. (2017). Cyclic Behavior of a Dense Nonplastic Silt.4th International Conference on Earthquake Engineering and Seismology (4ICEES), Anadolu University, Eskisehir, Turkey.

Tayfur G, Nadiri AA, Moghaddam AA. (2014). Supervised intelligent committee machine method for hydraulic conductivity estimation, Water resources management, 28(4), 1173-1184.

Tekin, E., & Akbas, S. O. (2019). Predicting groutability of granular soils using adaptive neuro-fuzzy inference system. Neural Computing and Applications, 31(4), 1091-1101002E

Thevanayagam S, Fiorillo M, Liang J. (2000). Effect of non-plastic fines on undrained cyclic strength of silty sands. In: Pak RYS, Yamamura J, editors. Soil Dynamics and Liquefaction 2000. Proceedings of Sessions of Geo-Denver 2000. ASCE Geotechnical Special Publication, vol. 107.; pp. 77–91.

Vaid, Y. P., & Thomas, J. (1995). Liquefaction and postliquefaction behavior of sand. Journal of Geotechnical Engineering, 121(2), 163-173.

Viviescas, J.C., Osorio, J.P. & Griffiths, D.V. Cluster analysis for the determination of the undrained strength tendency from SPT in mudflows and residual soils. Bull EngGeol Environ 78, 5039–5054 (2019). https://doi.org/10.1007/s10064-019-01472-8

Wang, S., Luna, R., & Onyejekwe, S. (2015). Post liquefaction behavior of low-plasticity silt at various degrees of reconsolidation. Soil Dynamics and Earthquake Engineering, 75, 259-264.

Wijewickreme, D., & Sanin, M. V. (2010). Post cyclic reconsolidation strains in low-plastic Fraser River silt due to dissipation of excess pore-water pressures. Journal of geotechnical and geoenvironmental engineering, 136(10), 1347-1357.

Xenaki VC, Athanasopoulos, GA. (2003). Liquefaction resistance of sand–silt mixtures: an experimental investigation of the effect of fines. Soil Dyn. Earthq. Eng. 23:183–94.

Yasuhara K, Murakami S, Komine H, Unno T. (2005). Effect of initial static shear stress and principal stress reversal on cyclic and post-cyclic undrained shear of sand. 16th ICSMGE, Osaka, Japan; 459-463.

Yasuhara K., & Andersen, K. H. (1991). Recompression of normally consolidated clay after cyclic loading. Soils and Foundations, 31(1), 83-94.

Yasuhara K., Hirao, K., & Hyde A. F. (1992). Effects of cyclic loading on undrained strength and compressibility of clay. Soils and Foundations, 32(1), 100-116.

Yoshida N, Yasuda S, Kiku M, Masuda T, Finn L. (1994). Behavior of sand after liquefaction. Proceedings from the fifth U.S.-Japan workshop on earthquake resistant design of lifeline facilities and countermeasures against soil liquefaction, Buffalo, N.Y., U.S. p.181–198.

Yoshimine M, Koike R. (2005). Liquefaction of clean sand with stratified structure due to segregation of particle size. Soils Found, 45:89–98.

Young F. J., & Hammer R. D. (2000). Defining geographic soil bodies by landscape position, soil taxonomy, and cluster analysis. Soil Science Society of America Journal, 64(3), 989-998.

Zhang W., Goh A. T., Zhang Y., Chen Y. & Xiao Y. (2015). Assessment of soil liquefaction based on capacity energy concept and multivariate adaptive regression splines. Engineering Geology, 188, 29-37.

Zhang Z, Tumay MT. (2003). Non-traditional approaches in soil classification derived from the cone penetration test. ASCE Geotechnic SpecialPubl.;121:101–49.